Feature
Article

phys. stat. sol. (b) **243**, No. 5, 1121–1138 (2006) / **DOI** 10.1002/pssb.200642005

Feature Article

Real-time, real-space implementation of the linear response time-dependent density-functional theory

K. Yabana[*, 1, 2], **T. Nakatsukasa**[1, 2], **J.-I. Iwata**[1], and **G. F. Bertsch**[3]

[1] Center for Computational Sciences, University of Tsukuba, Tsukuba 305-8571, Japan
[2] Institute of Physics, University of Tsukuba, Tsukuba 305-8571, Japan
[3] Department of Physics and Institute for Nuclear Theory, University of Washington, Seattle 98195, USA

Received 5 January 2006, revised 11 February 2006, accepted 14 February 2006
Published online 29 March 2006

PACS 31.15.Ew, 31.15.Fx, 33.60.–q, 71.15.Mb, 79.60.Jv

We review our methods to calculate optical response of molecules in the linear response time-dependent density-functional theory. Three distinct formalisms which are implemented in the three-dimensional grid representation are explained in detail. They are the real-time method solving the time-dependent Kohn–Sham equation in the time domain, the modified Sternheimer method which calculates the response to an external field of fixed frequency, and the matrix eigenvalue approach. We also illustrate treatments of the scattering boundary condition, needed to accurately describe photoionization processes. Finally, we show how the real-time formalism for molecules can be used to determine the response of infinite periodic systems.

1 Introduction

The density functional theory (DFT) is now recognized as a central tool to describe materials from the first-principle. The application of the DFT is, however, limited to electronic ground state of materials. The time-dependent density-functional theory (TDDFT) is an extension of the static DFT and describe electronic dynamics under external field, such as electronic excitations, optical responses, and various collision phenomena [1, 2].

The applications of the TDDFT are divided into two classes. One is the linear response TDDFT in which physical observables are extracted from TDDFT in the perturbation theory. This class of applications includes calculations of linear optical properties and electronic excitations in molecules and solids. Often the calculations reproduce measurements with satisfactory accuracy in a simple adiabatic approximation in which the same exchange-correlation potential is used as that has been employed in the static calculation. The other set of applications is to nonlinear electronic dynamics induced by an intense external field that cannot be treated as a perturbation. This class of applications includes electronic response under intense laser field [3, 4] and collisions involving highly charged ions [5, 6].

We have developed numerical implementations of the TDDFT employing a three-dimensional (3D) uniform-grid representation. There are three distinct implementations: The most direct approach is to evolve the Kohn–Sham orbitals by solving the time-dependent Kohn–Sham (TDKS) equation in time domain [7]. This approach is necessary to describe collision phenomena, the latter class of applications

[*] Corresponding author: e-mail: yabana@nucl.ph.tsukuba.ac.jp, Phone: +81 29 853 4202, Fax: +81 29 853 4492

in the above classification. The real-time evolution is also very useful to extract linear optical properties. Second is the modified Sternheimer method which calculates response to an external field of fixed frequency[1]. Third is the eigenvalue approach. The matrix eigenvalue approach is adopted in most quantum chemistry calculations [9–16]. Here we derive the eigenvalue equation in real-space representation [17].

The outline of this article is as follows. In Section 2, we present a general framework of the linear response TDDFT in the response function formalism. In Section 3, computational methods are presented. After explaining the real-space grid representation and the real-time propagation method, three distinct implementations of the linear response TDDFT are explained. In Section 4, a treatment of the scattering boundary condition is discussed to describe photoionization processes. In Section 5, our numerical implementation is demonstrated taking photoabsorption cross section of ethylene molecule as example. In Section 6, the real-time method is extended to describe dielectric function of infinite periodic systems. Finally, the summary is presented in Section 7.

2 Linear response in time-dependent density-functional theory

The TDDFT is intended to describe the change of the electron density from that of the ground state induced by an external potential. In the linear response TDDFT, the density change is calculated in the first order perturbation theory. Physical quantities are then extracted from the time-varying part of the density. In this section, we summarize a basic framework of the linear response TDDFT employing the density–density response function.

For a weak external potential, $V_{\mathrm{ext}}(\boldsymbol{r},t)$, the density change is a linear functional of the external potential. We denote the electron density at time t as $n(\boldsymbol{r},t)$ and the density in the ground state as $n_0(\boldsymbol{r})$. The density–density response function, $\chi(\boldsymbol{r},\boldsymbol{r}',t-t')$, is introduced to relate the density change $\delta n(\boldsymbol{r},t) \equiv n(\boldsymbol{r},t) - n_0(\boldsymbol{r})$ with the external potential,

$$\delta n(\boldsymbol{r},t) = \int_{-\infty}^{t} \mathrm{d}t' \int \mathrm{d}\boldsymbol{r}' \chi(\boldsymbol{r},\boldsymbol{r}',t-t') V_{\mathrm{ext}}(\boldsymbol{r}',t') , \tag{1}$$

where we assume that the system is independent of time in the absence of the external potential.

For a quantum system described by the time-independent many-body Hamiltonian H, the density–density response function can be expressed as follows:

$$\chi(\boldsymbol{r},\boldsymbol{r}',t-t') = \frac{1}{i\hbar}\theta(t-t')\langle \Phi_0 | [\hat{n}(\boldsymbol{r},t), \hat{n}(\boldsymbol{r}',t')] | \Phi_0 \rangle , \tag{2}$$

where $\theta(t)$ is the step function and Φ_0 is the ground state wave function. $\hat{n}(\boldsymbol{r},t)$ is defined by $\hat{n}(\boldsymbol{r},t) = \mathrm{e}^{iHt/\hbar}\hat{n}(\boldsymbol{r})\,\mathrm{e}^{-iHt/\hbar}$, $\hat{n}(\boldsymbol{r})$ being a usual density operator, $\hat{n}(\boldsymbol{r}) = \sum_i \delta(\boldsymbol{r}_i - \boldsymbol{r})$, where $\boldsymbol{r}_i$ is the coordinate of i-th electron.

For a perturbation with a fixed frequency ω, the relevant response function is the Fourier transform of Eq. (2). We write the explicit expression of the response function in terms of the eigenenergies E_n and eigenfunctions Φ_n of the Hamiltonian H, $H\Phi_n = E_n\Phi_n$:

$$\begin{aligned}\chi(\boldsymbol{r},\boldsymbol{r}',\omega) &= \int_{-\infty}^{\infty} \mathrm{d}t\ \mathrm{e}^{i\omega t}\chi(\boldsymbol{r},\boldsymbol{r}',t) \\ &= \sum_n \frac{\langle \Phi_0|\hat{n}(\boldsymbol{r})|\Phi_n\rangle\langle\Phi_n|\hat{n}(\boldsymbol{r}')|\Phi_0\rangle}{\hbar\omega + i\eta - (E_n - E_0)} - \frac{\langle \Phi_0|\hat{n}(\boldsymbol{r}')|\Phi_n\rangle\langle\Phi_n|\hat{n}(\boldsymbol{r})|\Phi_0\rangle}{\hbar\omega + i\eta + (E_n - E_0)} ,\end{aligned} \tag{3}$$

where the sum over n extends all the excited states of the system. η expresses a small positive number. The density–density response function in the frequency representation thus includes information on the excited states: excitation energies as poles and the transition densities as residues.

[1] The modified Sternheimer method has also been extended to second- and third-order nonlinear optical responses [8]. This will not be discussed in this article.

Linear optical properties of finite systems are characterized by the frequency-dependent dipole polarizability. We consider a dipole field in ν-direction with frequency ω. The potential is given by $V_{\text{ext}}(\boldsymbol{r}, t) = eE_0 r_\nu \, \mathrm{e}^{-i\omega t}$ where r_ν is one of the Cartesian coordinates, x, y, z. The polarizability $\alpha_{\mu\nu}(\omega)$ relates the polarization in μ-direction, $p_\mu(t)$, with the electric field in ν-direction, $E_\nu(t) = E_0 \, \mathrm{e}^{-i\omega t}$:

$$p_\mu(t) = \int \mathrm{d}\boldsymbol{r} \, (-\mathrm{e}) \, r_\mu \, \delta n(\boldsymbol{r}, t) = \alpha_{\mu\nu}(\omega) \, E_\nu(t) \, . \tag{4}$$

Employing the density–density response function, we have

$$\alpha_{\mu\nu}(\omega) = -e^2 \int \mathrm{d}\boldsymbol{r} \, \mathrm{d}\boldsymbol{r}' \, r_\mu r_\nu' \chi(\boldsymbol{r}, \boldsymbol{r}', \omega) \, . \tag{5}$$

We should note that the poles of the dipole polarizability correspond to the excitation energies of the system.

We next consider a density change under an external potential in the TDDFT. In the TDDFT, the density change is usually described by the TDKS equation.

$$i\hbar \frac{\partial}{\partial t} \psi_i(\boldsymbol{r}, t) = \{ h_{\text{KS}}[n(t)] + V_{\text{ext}}(\boldsymbol{r}, t) \} \, \psi_i(\boldsymbol{r}, t) \, , \tag{6}$$

where the Kohn–Sham Hamiltonian $h_{\text{KS}}[n(t)]$ is given by

$$h_{\text{KS}}[n(t)] = -\frac{\hbar^2}{2m} \nabla^2 + V_{\text{ion}}(\boldsymbol{r}) + \int \mathrm{d}\boldsymbol{r}' \, \frac{e^2}{|\boldsymbol{r} - \boldsymbol{r}'|} \, n(\boldsymbol{r}', t) + \mu_{\text{xc}}[n(\boldsymbol{r}, t)] \, , \tag{7}$$

and the time-dependent density is expressed in terms of the Kohn–Sham orbitals as

$$n(\boldsymbol{r}, t) = \sum_i | \psi_i(\boldsymbol{r}, t) |^2 \, . \tag{8}$$

The exchange-correlation potential $\mu_{\text{xc}}[n(\boldsymbol{r}, t)]$ is now a functional of the time-dependent density. This can be nonlocal in both space and time. If the exact functional is employed, we expect that the time-dependent density $n(\boldsymbol{r},t)$ calculated by the TDKS equation coincides with that in the exact many-body quantum theory [1]. In practice, a simple adiabatic approximation, in which the static exchange-correlation potential is used in the time-dependent problems, is often employed and is known to provide reasonable description for molecules. In some cases, a gradient correction [18] is employed and is known to provide a better description for excitations close to the ionization threshold and photoionization cross sections [10].

To proceed a perturbative treatment, we first make an expansion of the Kohn–Sham Hamiltonian up to a linear order in the density change around the density in the ground state. In the adiabatic local-density approximation (ALDA), we have

$$h_{\text{KS}}[n(\boldsymbol{r}, t)] = h_{\text{KS}}[n_0(\boldsymbol{r})] + \int \mathrm{d}\boldsymbol{r}' \, \frac{\delta h_{\text{KS}}[n(\boldsymbol{r})]}{\delta n(\boldsymbol{r}')} \, \delta n(\boldsymbol{r}', t) \, , \tag{9}$$

where the functional derivative of the Kohn–Sham Hamiltonian, $\delta h_{\text{KS}}/\delta n$, has the following form,

$$\frac{\delta h_{\text{KS}}[n(\boldsymbol{r})]}{\delta n(\boldsymbol{r}')} = \frac{e^2}{|\boldsymbol{r} - \boldsymbol{r}'|} + \frac{\delta \mu_{\text{xc}}[n(\boldsymbol{r})]}{\delta n} \, \delta(\boldsymbol{r} - \boldsymbol{r}') \, . \tag{10}$$

The potential, $(\delta h_{\text{KS}}/\delta n) \, \delta n(t)$, includes a dynamical screening effect induced by the change of the electron density. If we regard a sum of the external potential and the induced potential as a perturbation, one may describe the response of the system in terms the density–density response function without two-body interaction which we call the independent-particle response function and denote as $\chi_0(\boldsymbol{r}, \boldsymbol{r}', t - t')$. The density change is expressed as

$$\delta n(\boldsymbol{r}, t) = \int_{-\infty}^{t} \mathrm{d}t' \int \mathrm{d}\boldsymbol{r}' \chi_0(\boldsymbol{r}, \boldsymbol{r}', t - t') \left\{ V_{\text{ext}}(\boldsymbol{r}', t') + \int \mathrm{d}\boldsymbol{r}'' \, \frac{\delta h_{\text{KS}}[n(\boldsymbol{r}')]}{\delta n(\boldsymbol{r}'')} \, \delta n(\boldsymbol{r}'', t') \right\} . \tag{11}$$

For a perturbation with a fixed frequency ω, we can again separate the time variable. Expressing $\delta n(\boldsymbol{r}, t)$ as $\delta n(\boldsymbol{r})\,\mathrm{e}^{-i\omega t}$ and $V_{\mathrm{ext}}(\boldsymbol{r}, t)$ as $V_{\mathrm{ext}}(\boldsymbol{r})\,\mathrm{e}^{-i\omega t}$, we have

$$\delta n(\boldsymbol{r}) = \int \mathrm{d}\boldsymbol{r}'\, \chi_0(\boldsymbol{r}, \boldsymbol{r}', \omega) \left\{ V_{\mathrm{ext}}(\boldsymbol{r}') + \int \mathrm{d}\boldsymbol{r}''\, \frac{\delta h[n(\boldsymbol{r}')]}{\delta n(\boldsymbol{r}'')]}\, \delta n(\boldsymbol{r}'') \right\}. \tag{12}$$

This equation should be solved for $\delta n(\boldsymbol{r})$ at each frequency ω.

An explicit form of the independent-particle response function is given by

$$\chi_0(\boldsymbol{r}, \boldsymbol{r}', \omega) = \sum_{i \in \mathrm{occ.}} \sum_{m \in \mathrm{unocc.}} \left\{ \frac{\phi_i(\boldsymbol{r})\, \phi_m^*(\boldsymbol{r})\, \phi_m(\boldsymbol{r}')\, \phi_i^*(\boldsymbol{r}')}{\varepsilon_i - \varepsilon_m - \hbar\omega - i\eta} + \frac{\phi_i^*(\boldsymbol{r})\, \phi_m(\boldsymbol{r})\, \phi_m^*(\boldsymbol{r}')\, \phi_i(\boldsymbol{r}')}{\varepsilon_i - \varepsilon_m + \hbar\omega + i\eta} \right\}, \tag{13}$$

ϕ_i and ϕ_m are occupied and unoccupied Kohn–Sham orbitals with eigenenergies ε_i and ε_m, respectively.

The dipole polarizability in the TDDFT can be defined in the same way as in Eq. (4). To calculated it, we first set the external potential as $V_{\mathrm{ext}}(\boldsymbol{r}) = r_v$. Then $\delta n(\boldsymbol{r})$ is solved at each frequency ω. We obtain the polarizability by $\alpha_{\mu\nu}(\omega) = -e^2 \int \mathrm{d}\boldsymbol{r}\, r_\mu\, \delta n(\boldsymbol{r})$.

3 Computational methods

Calculations of the optical response with linear response TDDFT have been first achieved in early 80's for spherical systems, atoms [19] and metallic clusters [20]. Because the independent-particle response function χ_0 defined by Eq. (13) is a scalar integral kernel for spherical systems, Eq. (12) for $\delta n(\boldsymbol{r})$ is separated for each multipole component. The equation in each multipole is an integral equation of radial variable only, and can easily be solved numerically.

For systems without spherical symmetry, on the other hand, an explicit construction of the independent-particle response function (13) is numerically demanding, since it is a function of two coordinate variables $\boldsymbol{r}$ and $\boldsymbol{r}'$. This is especially true in the grid representation approaches such as the plane-wave basis expansion and the coordinate grid representation. For this reason, several efficient computational approaches have been developed which avoid explicit construction of the response function. In this section, we explain three approaches which are especially suited to the calculations in the 3D Cartesian grid representation. We first explain briefly the 3D Cartesian grid representation of the Kohn–Sham orbitals and then explain three implementations of the linear response TDDFT in the 3D grid representation.

3.1 3D Cartesian grid representation

Among various numerical methods to solve the Kohn–Sham equation in the electronic structure calculations, the finite difference method in the 3D Cartesian coordinate is a relatively new one [21, 22]. In the method, the 3D Cartesian coordinates are uniformly discretized. Usually only valence electrons are treated and the electron-ion interaction is replaced with the norm-conserving pseudopotential [23]. Expressing discretized Cartesian coordinates as $x_l = lh$, $y_m = mh$, $z_n = nh$ where h is the grid spacing and l, m, n are integers, the discretized Kohn–Sham equation has the following form

$$-\frac{\hbar^2}{2m} \sum_{l',m',n'} C_{l',m',n'} \phi_i(x_l + hl', y_m + hm', z_n + hn') + V_{\mathrm{loc}}(x_l, y_m, z_n)\, \phi_i(x_l, y_m, z_n)$$

$$+ \sum_{l'm'n'} V_{\mathrm{nonloc}}(x_l, y_m, z_n; x_{l'}, y_{m'}, z_{n'})\, \phi_i(x_{l'}, y_{m'}, z_{n'}) = \varepsilon_i \phi_i(x_l, y_m, z_n). \tag{14}$$

The local potential V_{loc} includes Hartree potential, exchange-correlation potential, and a local part of the ionic potential, while the nonlocal potential V_{nonloc} comes from nonlocal part of the pseudopotential for which we employ the separable approximation [24].

To decrease the number of grid points while keeping high numerical accuracy, one should employ a high-order finite difference formula for the kinetic energy operator [21, 22]. We usually employ the 9-point formula for each Cartesian coordinate.

The matrix dimension of the Kohn–Sham Hamiltonian is equal to the number of grid points in the 3D grid representation. Although the matrix dimension is usually very large, most of the off-diagonal elements are zero. For each row, the number of off-diagonal elements coming from the Laplacian is 25 in the 9-point formula, and that coming from the nonlocal part of the pseudopotential is typically 100–200 for each ion. In the methods explained below, an operation of the Kohn–Sham Hamiltonian on a wave function will appear frequently. This is a multiplication of a sparse matrix on a vector in the 3D grid representation.

3.2 Real-time evolution of the wave function

One of the methods to be explained below employs a real-time evolution of the Kohn–Sham orbitals. We briefly explain here how to solve the TDKS equation in real-time in the 3D grid representation.

Although the Kohn–Sham Hamiltonian is time-dependent, we may ignore the time dependence for a short period. Then the time evolution from t to $t+\Delta t$ may be computed using the Hamiltonian at t,

$$\psi_i(t+\Delta t) = \mathrm{e}^{-ih_{\mathrm{KS}}(t)\,\Delta t/\hbar}\,\psi_i(t)\,. \tag{15}$$

Several efficient schemes are known to evolve the wave function for a short period. We have been using a Taylor expansion method [7] which was originally used in the nuclear time-dependent Hartree–Fock calculation [25, 26]. In this method, the time evolution operator is expanded in the Taylor series, and the series is cut at a certain degree.

$$\psi_i(t+\Delta t) \simeq \sum_{k=0}^{k_{\max}} \frac{1}{k!}\left(\frac{-ih_{\mathrm{KS}}(t)}{\hbar}\right)^k \psi_i(t)\,. \tag{16}$$

The stability of the algorithm depends on $k_{\max}$ [27] as well as the time step Δt. We use the fourth order expansion, $k_{\max}=4$, which is stable for Δt smaller than $2.8\hbar/\varepsilon_{\max}$ where $\varepsilon_{\max} \sim 3\dfrac{\hbar^2}{2m}\left(\dfrac{\pi}{h}\right)^2$ is the maximum eigenvalue of the Hamiltonian h_{KS}.

The time evolution by the Taylor expansion method is not exactly unitary. However, we have found the orthonormalization of the orbitals are kept very accurate without explicit orthonormalization during the time evolution. For very long iteration, however, the breakdown of the orthonormalization becomes problematic. Such problems start to happen if one continues iteration typically 10^5 steps and more. We note that there has been proposed a method with unitarity employing a high-order Suzuki–Trotter formula in the plane wave basis [28]. We also note that the alternative leapfrog integration method is explicitly unitary if the Hamiltonian can be considered fixed as in Eq. (15) [27].

The approximation inherent in Eq. (15) may be improved by using the predictor-corrector method [25]. In the method, a density at a time $t+\Delta t$ is estimated once by Eq. (16). The density at a time $t+\Delta t/2$ is then approximated by $(n(t)+n(t+\Delta t/2))/2$. Then the Hamiltonian $h_{\mathrm{KS}}[(n(t)+n(t+\Delta t))/2]$ is used in the time evolution instead of $h_{\mathrm{KS}}[n(t)]$ in Eq. (16). This prescription of the predictor-corrector step makes a time evolution more accurate. For example, the energy is better conserved in the absence of the external potential with the predictor-corrector step than that without the step. However, we found that the dipole moment $p_\mu(t)$,which is related to the polarizability by Fourier transformation, changes little by the addition of the predictor-corrector step.

3.3 A real-time method

The most direct way to calculate the polarizability is to solve the TDKS equation in real time. As explained in Eq. (4), the dipole polarizability $\alpha_{\mu\nu}(\omega)$ is defined as a coefficient between the induced polari-

zation $p_\mu(t)$ and the applied external electric field $E(t)$ of a fixed frequency ω applied to ν direction, $E(t) = E_0\, \mathrm{e}^{-i\omega t}$. Now let us consider an induced dipole moment p_μ for an electric field of arbitrary time profile in ν-direction, $V_{\mathrm{ext}}(\boldsymbol{r}, t) = eE(t)\, r_\nu$, either in full many-body dynamics or in TDKS dynamics. In the linear response regime, each ω component of $p_\mu(t)$ and $E(t)$ should be related by the dipole polarizability $\alpha_{\mu\nu}(\omega)$ since there holds a principle of superposition,

$$\int \mathrm{d}t\, \mathrm{e}^{i\omega t}\, p_\mu(t) = \alpha_{\mu\nu}(\omega) \int \mathrm{d}t\, \mathrm{e}^{i\omega t}\, E(t)\,, \tag{17}$$

This relation tells us that, for an applied electric field of any time profile, we can calculate the dipole polarizability by taking a ratio of the Fourier transforms,

$$\alpha_{\mu\nu}(\omega) = \frac{1}{\tilde{E}(\omega)} \int \mathrm{d}t\, \mathrm{e}^{i\omega t}\, p_\mu(t)\,, \tag{18}$$

where $\tilde{E}(\omega)$ is the Fourier transform of the applied electric field, $\tilde{E}(\omega) = \int \mathrm{d}t\, \mathrm{e}^{i\omega t}\, E(t)$.

There are two simple and useful choices for the time profile of the electric field. One is the impulsive electric field [7] in which the potential is expressed as

$$V_{\mathrm{ext}}(\boldsymbol{r}, t) = I\, \delta(t)\, r_\nu\,, \tag{19}$$

where I is the magnitude of the impulse. In the classical mechanics, all the electrons in the system get an initial velocity $v = I/m$ by this impulse. In the quantum mechanics, every orbital is multiplied with the plane wave with momentum I. This is understood as follows. Before the impulsive force is applied, the system is in the ground state described by the static Kohn–Sham orbitals. The orbitals before and after the impulsive force is related by the time evolution operator,

$$\psi_i(t_{0+}) = \exp\left\{ \frac{i}{\hbar} \int_{0-}^{0+} \mathrm{d}t\, (h_{\mathrm{KS}}[n_0] + I\, \delta(t)\, r_\nu) \right\} \psi_i(t_{0-})\,. \tag{20}$$

For a small time interval, the Kohn–Sham Hamiltonian in the time evolution operator may be ignored. Thus the orbitals just after the impulsive force are given by

$$\psi_i(\boldsymbol{r}, t = 0_+) = \mathrm{e}^{ikr_\nu}\, \phi_i(\boldsymbol{r})\,, \tag{21}$$

where k is given by $k = I/\hbar$.

Starting with this initial wave function, we evolve the orbitals without any external potential. The dipole moment is calculated from the orbitals by $d_\mu(t) = \int \mathrm{d}\boldsymbol{r}\, r_\mu \sum_i |\psi_i(\boldsymbol{r}, t)|^2$. The Fourier transform of the impulse field is just a constant. The polarizability is calculated by

$$\alpha_{\mu\nu}(\omega) = -\frac{e^2}{I} \int_0^\infty \mathrm{d}t\, \mathrm{e}^{i\omega t}\, d_\mu(t)\,. \tag{22}$$

Since the impulsive field includes all the frequency component uniformly, we may obtain the polarizability for a whole spectral region from a single time evolution.

Another simple choice is to apply a static uniform field at $t > 0$,

$$E(t) = \begin{cases} 0 & (t < 0) \\ E_0 & (t > 0) \end{cases}. \tag{23}$$

The Fourier transform is given by $\tilde{E}(\omega) = -E_0/i\omega$. Before $t = 0$, the system is again in the ground state described by the static Kohn–Sham orbitals. After the electric field is switched on, the polarization oscil-

lates around a static polarization p_μ^0 which is related to the static polarizability by $p_\mu^0 = \alpha_{\mu\nu}(0)E_0$. The polarizability can be obtained from the induced polarization,

$$\alpha_{\mu\nu}(\omega) = -\frac{i\omega}{E_0}\int_0^{+\infty} \mathrm{d}t\, \mathrm{e}^{i\omega t}\, p_\mu(t)\,. \tag{24}$$

A transition to bound excited state appears as a delta function in the imaginary part of the polarizability. In practice, the time evolution is carried out for a finite period T. The energy resolution of the spectrum ΔE obtained by the Fourier transform is related to the time period T by the uncertainly principle, $\Delta E \sim h/T$.

In the polarization $p_\mu(t)$, transitions to bound excited states appear as oscillations which persist without any damping. The Fourier transform of such oscillation in finite period accompanies wiggles around the excitation energy because of the abrupt cut of the oscillation. The wiggles can be eliminated to some extent by introducing a damping function in the Fourier transformation. A simple choice for the damping function is to include a small imaginary part $i\gamma$ in the frequency ω. This is equivalent to multiply a damping function

$$f(t) = \mathrm{e}^{-\gamma t}\,, \tag{25}$$

in the Fourier transform of Eq. (18). This gives the bound transitions a Lorentzian line shape, if the time evolution is achieved for sufficiently long period.

Another choice which we often employ is the following damping function which is a third order polynomial in time,

$$f(t) = 1 - 3\left(\frac{t}{T}\right)^2 + 2\left(\frac{t}{T}\right)^3. \tag{26}$$

This function has the following properties: $f(0) = 1$, $f'(0) = f'(T) = f'(T) = 0$. The conditions $f(T) = f'(T) = 0$ make the polarization $p_\mu(t)$ vanish smoothly at $t = T$. The condition $f'(0) = 0$ guarantees that the integral of the oscillator strength, namely the Thomas–Reiche–Kuhn sum rule, is not changed by introducing the damping function. Using Eq. (26) for the damping factor, the line width (FWHM) is found to be $\Gamma_{\mathrm{FWHM}} \approx 6.2\hbar/T$.

We note several characteristic features of the real-time method. First, we never need to calculate unoccupied Kohn–Sham orbitals. The information of the unoccupied orbitals come in through the time evolution of the Kohn–Sham orbitals. Since we only calculate time evolution of the occupied orbitals, the memory requirement in the calculation is just as twice as the static Kohn–Sham calculation. The factor 2 comes from the complex orbitals in the TDKS calculation while the orbitals are real in the static calculation. Second, we can obtain a spectrum of whole frequency region from a single time evolution. On the other hand, even when one is interested in a certain low-lying transition, we need to achieve time evolution for a long period. Third, the computational algorithm is quite simple. As noted in the previous subsection, the time evolution can be achieved by applying the Kohn–Sham Hamiltonian several times to the orbitals. Therefore, no additional coding is necessary except for the the operation of the Kohn–Sham Hamiltonian to a certain wave function.

3.4 Modified Sternheimer method

We next consider a response to an external potential of fixed frequency. This was considered in Section 2, and Eq. (12) should be solved for $\delta n(\boldsymbol{r})$. However, the explicit construction of $\chi_0(\boldsymbol{r},\boldsymbol{r}',\omega)$ is not easy in the 3D grid representation. There is a method called the modified Sternheimer method [29–33] in which the explicit construction of the response function may be avoided [8, 34]. It is also not necessary to calculate unoccupied orbitals, as in the real-time method. We here outline the method.

We first express the TDKS orbital ψ_i as a sum of the static Kohn–Sham orbital ϕ_i and the small deviation $\delta\psi_i$,

$$\psi_i(\boldsymbol{r},t) = \left(\phi_i(\boldsymbol{r}) + \delta\psi_i(\boldsymbol{r},t)\right) \mathrm{e}^{-i\varepsilon_i t/\hbar} . \tag{27}$$

Substituting this expansion into the TDKS equation, we obtain the equation for $\delta\psi_i$ which is first order in the external potential,

$$i\hbar \frac{\partial}{\partial t} \delta\psi_i(\boldsymbol{r},t) = (h_0(\boldsymbol{r}) - \varepsilon_i) + \left(\int \mathrm{d}\boldsymbol{r}' \, \frac{\delta h_{\mathrm{KS}}[n(\boldsymbol{r})]}{\delta n(\boldsymbol{r}')} \delta n(\boldsymbol{r}',t) + V_{\mathrm{ext}}(\boldsymbol{r},t) \right) \phi_i(\boldsymbol{r}) . \tag{28}$$

Here we express the static Kohn–Sham Hamiltonian as $h_0(\boldsymbol{r})$. The density change $\delta n(\boldsymbol{r},t)$ is expressed as

$$\delta n(\boldsymbol{r},t) = \sum_{i\in\mathrm{occ}} \phi_i^*(\boldsymbol{r}) \, \delta\psi_i(\boldsymbol{r},t) + \phi_i(\boldsymbol{r}) \, \delta\psi_i^*(\boldsymbol{r},t) . \tag{29}$$

We consider an external potential with a fixed frequency ω, $V_{\mathrm{ext}}(\boldsymbol{r},t) = V_{\mathrm{ext}}(\boldsymbol{r}) \, \mathrm{e}^{-i\omega t} + V_{\mathrm{ext}}^*(\boldsymbol{r}) \, \mathrm{e}^{i\omega t}$. Then we can separate time variable by putting $\delta\psi_i$ as

$$\delta\psi_i(\boldsymbol{r},t) = \delta\psi_i^{(+)}(\boldsymbol{r}) \, \mathrm{e}^{-i\omega t} + \delta\psi_i^{(-)}(\boldsymbol{r}) \, \mathrm{e}^{i\omega t} . \tag{30}$$

The equations for $\delta\psi_i^{(+)}(\boldsymbol{r})$ and $\delta\psi_i^{(-)}(\boldsymbol{r})$ are given by

$$\hbar\omega \, \delta\psi_i^{(+)}(\boldsymbol{r}) = (h_0(\boldsymbol{r}) - \varepsilon_i) \, \delta\psi_i^{(+)}(\boldsymbol{r}) + \phi_i(\boldsymbol{r}) \int \mathrm{d}\boldsymbol{r}' \, \frac{\delta h_{\mathrm{KS}}[n(\boldsymbol{r})]}{\delta n(\boldsymbol{r}')} \delta n(\boldsymbol{r}') + V_{\mathrm{ext}}(\boldsymbol{r}) \, \phi_i(\boldsymbol{r}) , \tag{31}$$

$$-\hbar\omega \, \delta\psi_i^{(-)}(\boldsymbol{r}) = (h_0(\boldsymbol{r}) - \varepsilon_i) \, \delta\psi_i^{(-)}(\boldsymbol{r}) + \phi_i(\boldsymbol{r}) \int \mathrm{d}\boldsymbol{r}' \, \frac{\delta h_{\mathrm{KS}}[n(\boldsymbol{r})]}{\delta n(\boldsymbol{r}')} \delta n^*(\boldsymbol{r}') + V_{\mathrm{ext}}^*(\boldsymbol{r}) \, \phi_i(\boldsymbol{r}) , \tag{32}$$

where $\delta n(\boldsymbol{r})$ is related to $\delta n(\boldsymbol{r},t)$ by

$$\delta n(\boldsymbol{r},t) = \delta n(\boldsymbol{r}) \, \mathrm{e}^{-i\omega t} + \delta n^*(\boldsymbol{r}) \, \mathrm{e}^{i\omega t} . \tag{33}$$

We call $\delta n(\boldsymbol{r})$ as a transition density associated with the frequency ω. It is expressed in terms of the wave functions,

$$\delta n(\boldsymbol{r}) = \sum_i \phi_i^*(\boldsymbol{r}) \, \delta\psi_i^{(+)}(\boldsymbol{r}) + \phi_i(\boldsymbol{r}) \, \delta\psi_i^{(-)*}(\boldsymbol{r}) . \tag{34}$$

Equations (31) and (32) are linear equations for $\delta\psi_i^{(\pm)}(\boldsymbol{r})$. This fact is more clearly seen by rewriting them in the following matrix form,

$$\left\{ \hbar\omega \begin{pmatrix} \boldsymbol{I} & 0 \\ 0 & -\boldsymbol{I} \end{pmatrix} - \begin{pmatrix} \boldsymbol{A} & \boldsymbol{B} \\ \boldsymbol{B}^* & \boldsymbol{A}^* \end{pmatrix} \right\} \begin{pmatrix} \delta\psi^{(+)} \\ \delta\psi^{(-)*} \end{pmatrix} = V_{\mathrm{ext}} \begin{pmatrix} \phi \\ \phi^* \end{pmatrix} . \tag{35}$$

The dimension of the matrix is twice of the number of occupied orbitals, and the integral over coordinate is assumed. $\boldsymbol{I}$ is a unit operator, diagonal matrix in the orbital indices and the delta function in the coordinate, $\boldsymbol{I} = \delta_{ij} \, \delta(\boldsymbol{r} - \boldsymbol{r}')$. $\delta\psi^{(\pm)}$ and ϕ are column vectors whose components are functions $\delta\psi_i^{(\pm)}(\boldsymbol{r})$ and $\phi_i(\boldsymbol{r})$, respectively. $\boldsymbol{A}$ and $\boldsymbol{B}$ are matrices whose dimension is equal to the number of occupied orbitals, and each component is the integral kernel,

$$\boldsymbol{A}_{ij} = (h_0(\boldsymbol{r}) - \varepsilon_i) \, \delta(\boldsymbol{r} - \boldsymbol{r}') \, \delta_{ij} + \phi_i(\boldsymbol{r}) \, \frac{\delta h(\boldsymbol{r})}{\delta n(\boldsymbol{r}')} \, \phi_j^*(\boldsymbol{r}') , \tag{36}$$

$$\boldsymbol{B}_{ij} = \phi_i(\boldsymbol{r}) \, \frac{\delta h(\boldsymbol{r})}{\delta n(\boldsymbol{r}')} \, \phi_j(\boldsymbol{r}') . \tag{37}$$

Equation (35) is the equation of linear response TDDFT for a fixed frequency, convenient for computation in the 3D grid representation. To obtain dipole polarizability, the potential is set to $V_{\mathrm{ext}}(\boldsymbol{r}) = r_\nu$. For each frequency ω, Eq. (35) is solved repeatedly to calculate $\delta\psi_i^{(+)}$ and $\delta\psi_i^{(-)}$. The density $\delta n(\boldsymbol{r})$ is then constructed by Eq. (34). The polarizability is calculated from the density $\delta n(\boldsymbol{r})$ by $\alpha_{\mu\nu}(\omega) = -e^2 \int \mathrm{d}\boldsymbol{r}\; r_\mu\, \delta n(\boldsymbol{r})$. In the 3D grid representation, Eq. (35) is a linear algebraic equation. We found the equation can be efficiently solved by iterative procedures such as the conjugate gradient method [8].

3.5 Eigenvalue problem

In the absence of the external potential, Eq. (35) can be regarded as an eigenvalue problem in which the eigenvalues $\hbar\omega$ provide excitation energies [17]. In the 3D grid representation, the dimension of the matrix is $2N_x N_{\mathrm{orb}}$ where N_x is the number of grid points and N_{orb} is the number of occupied orbitals. The number of the eigenvalues is equal to the number of this dimension. The eigenvalues of this equation appear in a pair, $\pm\hbar\omega$. Suppose that $\hbar\omega_n$ is an eigenvalue with the eigenvector $(\delta\psi_i^{[n](+)}, \delta\psi_i^{[n](-)*})$. Then it can be easily seen that the eigenvector belonging to the eigenvalue $-\hbar\omega$ is given by $(\delta\psi_i^{[n](-)}, \delta\psi_i^{[n](+)*})$. Only positive eigenenergies are physically relevant, and the number of physical eigenmodes is $N_x N_{\mathrm{orb}}$.

The equation in the 3D grid representation has a form of generalized eigenvalue problem. Again, the conjugate gradient method works well to obtain a few low-lying eigenvalues and eigenvectors. For each excitation, we need to store $\delta\psi_i^{(+)}(\boldsymbol{r})$ and $\delta\psi_i^{(-)}(\boldsymbol{r})$. To calculate several low-lying excitations, we need to find solution imposing orthogonality to other excited states which have been already obtained. Therefore, for each excitation, the memory requirement is two times that for the static calculation.

The eigenvalue problem approach is well suited to calculate very accurate solution for a few low-lying excitations. We have applied this approach to investigate electron-ion coupling [35, 36].

A more familiar form of the eigenvalue equation is the particle-hole representation which is obtained from the coordinate representation by expanding the unknown orbitals $\psi_i^{(+)}$ and $\psi_i^{(-)}$ in terms of the static Kohn–Sham orbitals,

$$\psi_i^{(+)}(\boldsymbol{r}) = \sum_m X_{im}\phi_m(\boldsymbol{r}), \tag{38}$$

$$\psi_i^{(-)}(\boldsymbol{r}) = \sum_n Y_{in}^*\phi_n(\boldsymbol{r}), \tag{39}$$

where, in the sum over m and n, only unoccupied orbitals are necessary. The eigenvalue equation is expressed as

$$\begin{pmatrix} \boldsymbol{A} & \boldsymbol{B} \\ \boldsymbol{B}^* & \boldsymbol{A}^* \end{pmatrix} \begin{pmatrix} \boldsymbol{X} \\ \boldsymbol{Y}^* \end{pmatrix} = \hbar\omega \begin{pmatrix} \boldsymbol{X} \\ -\boldsymbol{Y}^* \end{pmatrix}, \tag{40}$$

where $\boldsymbol{A}$ and $\boldsymbol{B}$ are defined by

$$A_{im,jn} = (\varepsilon_m - \varepsilon_i)\,\delta_{mn}\delta_{ij} + \left\langle \phi_m\phi_j \left| \frac{\delta h}{\delta n} \right| \phi_i\phi_n \right\rangle, \tag{41}$$

$$B_{im,jn} = \left\langle \phi_m\phi_n \left| \frac{\delta h}{\delta n} \right| \phi_i\phi_j \right\rangle. \tag{42}$$

The dimension of the eigenvalue problem is $2N_{\mathrm{occ}}N_{\mathrm{unocc}}$, where N_{unocc} is the number of unoccupied orbitals to be prepared. This method gains great efficiency when the orbital spaces $N_{\mathrm{occ}}, N_{\mathrm{unocc}}$ can be se-

verely truncated. This is the case for the calculation of the low-frequency dipole response of large systems below the photoionization threshold.

The matrix diagonalization in the particle-hole representation is a standard approach of TDDFT in the quantum chemistry calculations [9–16]. In these calculations, Eq. (40) is solved after transforming it to an Hermite eigenvalue problem of dimension $N_{\rm occ}N_{\rm unocc}$. The matrix diagonalization approach is also adopted in [37] employing the 3D grid representation to prepare occupied and unocupied orbitals.

4 Treatment of photoionization process

In finite systems, excited states are composed of discrete and continuum spectra. Above the ionization threshold, most of the photoabsorption cross section results in photoionization. To describe the process, scattering boundary condition must be imposed on the final state wave function. In the response function formalism, the boundary condition can be incorporated by expressing the independent-particle response function of Eq. (13) in terms of the Green's function with appropriate boundary conditions.

$$\chi_0(\boldsymbol{r},\boldsymbol{r}',\omega)=\sum_i\left\{\phi_i(\boldsymbol{r})\,G^{(-)}(\boldsymbol{r},\boldsymbol{r}',\varepsilon_i-\hbar\omega)\,\phi_i^*(\boldsymbol{r}')+\phi_i^*(\boldsymbol{r})\,G^{(+)}(\boldsymbol{r},\boldsymbol{r}',\varepsilon_i+\hbar\omega)\,\phi_i(\boldsymbol{r}')\right\}, \tag{43}$$

where the single-particle Green's function is defined by

$$G^{(\pm)}(\boldsymbol{r},\boldsymbol{r}',E)=\langle\boldsymbol{r}|\,(E-h_0\pm i\eta)^{-1}\,|\boldsymbol{r}'\rangle\,. \tag{44}$$

The superscript $+(-)$ indicates the outgoing (incoming) boundary condition.

For systems with spherical symmetry, the outgoing Green's function can easily be constructed in the multipole expansion.

$$G^{(\pm)}(\boldsymbol{r},\boldsymbol{r}',E)=\frac{2m}{\hbar^2}\sum_{lm}Y_{lm}(\hat{r})\,\frac{u_l(r_<)\,w_l^{(\pm)}(r_>)}{W[u_l,w_l^{(\pm)}]\,rr'}\,Y_{lm}^*(\hat{r}')\,, \tag{45}$$

where $u_l(r)$ and $w_l^{(\pm)}(r)$ are radial wave functions in the static Kohn–Sham Hamiltonian $h_0(\boldsymbol{r})$ at energy E. The $u_l(r)$ is a regular wave function and $w_l^{(\pm)}(r)$ are irregular wave functions with outgoing (+) and incoming (−) boundary conditions, respectively. The first TDDFT calculation for atoms and metallic clusters was achieved with this treatment for boundary condition [19, 20]. The same method has also been applied to the giant resonances of atomic nuclei [38].

To describe photoionization process for systems without spherical symmetry, we have developed two methods which are applicable in the 3D grid representation [34]. One is to impose the outgoing boundary condition approximately by placing an absorbing potential outside the molecule. This is applicable to both the real-time and the modified Sternheimer methods. The other is a more accurate approach which is applicable only in the modified Sternheimer approach. We explain both methods below.

4.1 Absorbing boundary condition approach

Let us consider photoionization process of molecules in the real-time calculation. When an external field is applied to the molecule, the Kohn–Sham orbitals are excited and include components corresponding to unbound orbitals of the static Kohn–Sham Hamiltonian. During the time evolution, electrons excited to the unbound orbital are emitted outside the molecule. Once the electron is emitted outside the molecule, it never returns to the region around the molecule. The electrons emitted outside do not contribute to the transition density and to the polarizability, since the density change $\delta n(\boldsymbol{r},t)$ given by Eq. (29) only includes terms which are products with the occupied Kohn–Sham orbitals.

In the 3D grid representation, we solve the TDKS equation inside a certain box area. In the time evolution, the electrons emitted to the continuum states are reflected at the box boundary, and return to the region of the molecule. The reflected wave makes a standing wave in the region of the molecule and

contributes to the polarizability. In other words, all the unoccupied orbitals become discrete states in the finite box-size calculation, and all the excitation spectra in the TDDFT are also discrete even above the ionization threshold. To describe ionization process adequately, one must remove electrons which are emitted outside the molecule during the time evolution.

An approximate removal of emitted electrons is feasible by placing an imaginary potential outside the molecule. In the presence of the negative imaginary potential, the flux is absorbed during the propagation. This is the so-called absorbing boundary condition (ABC) which has been originally developed in the field of atomic and molecular collisions [39, 41].

The absorbing potential should be smooth enough so that the flux getting into the region of the absorbing potential is not reflected. On the other hand, the absorbing potential should be strong enough so that the all the flux is absorbed efficiently. These two conditions may be satisfied if one employs a thick area of absorbing potential. This however increases the number of grid points to be employed. We must find a compromise of these conflicting conditions.

The absorbing potential with a linear coordinate dependence is often employed and the condition for a good absorber has been well investigated. The potential is placed at a spatial region where radial coordinate r is greater than a certain radius R beyond which the electron density in the ground state can be negligible. Denoting the thickness of the absorbing region as ΔR, the absorbing potential is placed in the region $R \le r \le R + \Delta R$,

$$-iW(r) = \begin{cases} 0 & (0 < r < R) \\ -iW_0 \dfrac{r-R}{\Delta R} & (R < r < R + \Delta R) \end{cases}. \tag{46}$$

The height W_0 and the width ΔR must be carefully chosen. The WKB analysis provides the following condition among parameters to be a good absorber [34],

$$20\frac{E^{1/2}}{\Delta r\sqrt{8m}} < |W_0| < \frac{1}{10}\Delta r\sqrt{8m}E^{3/2}, \tag{47}$$

where E is the energy of the particle that comes in in the region of the absorbing potential. The left inequality originates from the condition that the flux is well absorbed, while the right inequality from the condition that the flux is not reflected at by the absorber. In practice, the energy of the emitted electron is not unique. We first set the energy range for which we expect the absorbing potential works efficiently, and then find ΔR and W_0 which satisfy Eq. (47) for the energy range.

The absorbing potential method can be applied to both real-time method and the modified Sternheimer method. In the real-time method, the absorbing potential is simply added to the Kohn–Sham Hamiltonian in the time evolution,

$$i\hbar\frac{\partial}{\partial t}\psi_i(\boldsymbol{r},t) = \{h[n(t)] - iW(r) + V_{\text{ext}}(\boldsymbol{r},t)\}\psi_i(\boldsymbol{r},t). \tag{48}$$

In the presence of the absorbing potential, the time evolution is no more unitary. However, we have found that the time evolution is stable with the algorithm of Taylor expansion.

In the modified Sternheimer method, the absorbing potential is added to the static Kohn–Sham Hamiltonian $h_0(\boldsymbol{r})$ in Eq. (36). In this case, the energy transferred from the external field to the electron is a fixed value, $\hbar\omega$. However, the energy of the electron emitted to the continuum is $\hbar\omega + \varepsilon_i$, dependent on the orbital energy. In the presence of the absorbing potential, the coefficient matrix of Eq. (35) is no more hermite. In that case, a Bi-conjugate gradient method may work well to solve the equation.

4.2 Green's function method

We next consider a method to impose the outgoing boundary condition accurately in the modified Sternheimer formalism [34]. In Section 3.4, we stated that Eq. (35) should be solved to obtain $\delta\psi_i^{(\pm)}(\boldsymbol{r})$ and

then the transition density $\delta n(\boldsymbol{r})$ is calculated by Eq. (34). Here we consider the modified Sternheimer method in a slightly different way.

To describe ionization, the outgoing boundary condition should be imposed on $\psi_i^{(+)}(\boldsymbol{r})$. This is achieved by rewriting Eq. (31) as follows:

$$\delta\psi_i^{(+)}(\boldsymbol{r}) = \int \mathrm{d}\boldsymbol{r}'\, G^{(+)}(\boldsymbol{r},\boldsymbol{r}',\hbar\omega+\varepsilon_i)\, V_{\mathrm{scf}}(\boldsymbol{r}')\,\phi_i(\boldsymbol{r}')\,, \tag{49}$$

where the self-consistent potential including dynamical screening effect is given by

$$V_{\mathrm{scf}}(\boldsymbol{r}) = V_{\mathrm{ext}}(\boldsymbol{r}) + \int \mathrm{d}\boldsymbol{r}'\, \frac{\delta h_{\mathrm{KS}}[n(\boldsymbol{r})]}{\delta n(\boldsymbol{r}')}\,\delta n(\boldsymbol{r}')\,. \tag{50}$$

Since $\delta n(\boldsymbol{r})$ is given by Eq. (34) and is included in $V_{\mathrm{scf}}(\boldsymbol{r})$, these equations should be solved self-consistently for $\delta n(\boldsymbol{r})$. In the 3D grid representation, this is a linear algebraic problem for $\delta n(\boldsymbol{r})$ and can be solved by the iterative method. In the iterative procedure, one must calculate $\delta\psi_i^{(+)}(\boldsymbol{r})$ defined by Eq. (49) for a given potential $V_{\mathrm{scf}}(\boldsymbol{r})$.

Since we consider a case in which the static Kohn–Sham Hamiltonian $h_0(\boldsymbol{r})$ is not spherically symmetric, multipole expansion of the Green's function, Eq. (45), cannot be used. We instead utilize the integral equation for the Green's function. We first divide the potential in the static Kohn–Sham Hamiltonian into two: one is the local potential $V_0(r)$ which is spherically symmetric and may be long ranged. The other is the nonspherical potential which is short-ranged and may be non-local, $\tilde{V}(\boldsymbol{r},\boldsymbol{r}')$. Then there follows

$$G^{(+)}(\boldsymbol{r},\boldsymbol{r}';E) = G_0^{(+)}(\boldsymbol{r},\boldsymbol{r}';E) + \int \mathrm{d}\boldsymbol{r}''\,\mathrm{d}\boldsymbol{r}'''\, G_0^{(+)}(\boldsymbol{r},\boldsymbol{r}'';E)\,\tilde{V}(\boldsymbol{r}'',\boldsymbol{r}''')\,G^{(+)}(\boldsymbol{r}''',\boldsymbol{r}';E)\,, \tag{51}$$

where $G_0^{(+)}$ is the Green's function for the Hamiltonian involving the spherical potential $V_0(r)$. Employing this identity, Eq. (49) can be written in the following way,

$$\begin{aligned}&\delta\psi_i^{(+)}(\boldsymbol{r}) - \int \mathrm{d}\boldsymbol{r}'\,\mathrm{d}\boldsymbol{r}''\, G_0^{(+)}(\boldsymbol{r},\boldsymbol{r}';\hbar\omega+\varepsilon_i)\,\tilde{V}(\boldsymbol{r}',\boldsymbol{r}'')\,\delta\psi_i^{(+)}(\boldsymbol{r}'')\\ &= \int \mathrm{d}\boldsymbol{r}'\, G_0^{(+)}(\boldsymbol{r},\boldsymbol{r}';\hbar\omega+\varepsilon_i)\, V_{\mathrm{scf}}(\boldsymbol{r}')\,\phi_i(\boldsymbol{r}')\,.\end{aligned} \tag{52}$$

This is a linear algebraic equation for $\delta\psi^{(+)}(\boldsymbol{r})$ in the 3D grid representation, and we can solve it employing an iterative method. As part of the procedure, one must calculate integrals of the form

$$g(\boldsymbol{r}) = \int \mathrm{d}\boldsymbol{r}'\, G_0^{(+)}(\boldsymbol{r},\boldsymbol{r}';E)\, f(\boldsymbol{r}')\,, \tag{53}$$

where $f(\boldsymbol{r}) = V_{\mathrm{scf}}(\boldsymbol{r})\,\phi_i(\boldsymbol{r})$ and $f(\boldsymbol{r}) = \int \mathrm{d}\boldsymbol{r}'\,\tilde{V}(\boldsymbol{r},\boldsymbol{r}')\,\delta\psi_i^{(+)}(\boldsymbol{r}')$. We note that the function $f(\boldsymbol{r})$ is a short range function since it include occupied orbitals $\phi_i(\boldsymbol{r})$ or short range potential $\tilde{V}(\boldsymbol{r},\boldsymbol{r}')$. To calculate $g(\boldsymbol{r})$ from $f(\boldsymbol{r})$ in the 3D grid representation, we recast the equation into differential form,

$$\left\{E - \left(-\frac{\hbar^2}{2m}\nabla^2 + V_0(r)\right)\right\} g(\boldsymbol{r}) = f(\boldsymbol{r})\,. \tag{54}$$

This is a linear algebraic equation for $g(\boldsymbol{r})$ and is again solved by an iterative method. In the iterative procedure, the values of the function $g(\boldsymbol{r})$ outside the spatial area of grid points are required to evaluate the Laplacian operator in the grid points. Suppose that we employ grid points inside a spherical region of radius R. We prepare the boundary values of $g(\boldsymbol{r})$ outside the radius R by employing the multipole expansion of the Green's function $G_0^{(+)}$, Eq. (45). Namely, we first calculate the multipole moment of $f(\boldsymbol{r})$,

$$f_{lm} = \frac{2m}{\hbar^2}\,\frac{1}{W[u_l, w_l^{(+)}]}\int_{r<R} \mathrm{d}\boldsymbol{r}\,\frac{u_l(r)}{r}\,Y_{lm}^*(\hat{r})\, f(\boldsymbol{r})\,. \tag{55}$$

The function $g(\boldsymbol{r})$ outside the sphere is calculated by

$$g(\boldsymbol{r})|_{r>R} = \sum_{lm} f_{lm} \frac{w_l^{(+)}(r)}{r} Y_{lm}(\hat{r}) . \tag{56}$$

The Green's function method thus requires to solve multiple nested linear algebraic equations, which is summarized as follows. For the external potential $V_{\text{ext}}(\boldsymbol{r}) = r_v$, we solve the transition density $\delta n(\boldsymbol{r})$ which is given by Eqs. (49), (50), and a similar equation for $\delta\psi_i^{(-)}(\boldsymbol{r})$. This is the linear algebraic equation whose dimension is equal to N_{x}, the number of grid points. In the iterative procedure, we solve Eq. (52) for $\delta\psi_i^{(+)}(\boldsymbol{r})$ for a given self-consistent potential $V_{\text{scf}}(\boldsymbol{r})$. This is again a linear algebraic equation of dimension N_x for each occupied orbital index i. In this procedure, we need to evaluate the operation of the Green's function with spherical potential, Eq. (53). We achieve it by solving Eq. (54), which is again a linear algebraic equation of dimension N_x. In solving the linear algebraic equations, the conjugate gradient method and its variant offer a stable and efficient scheme.

5 Example: optical absorption of ethylene molecule

In this section, we demonstrate the numerical method presented in the previous sections taking the optical response of ethylene molecule as an example.

In Fig. 1, real-time calculations are shown employing electric fields of three different time profiles. In all cases, the electric field is applied to the direction of molecular axis involving two Carbon atoms. The polarization is calculated along the same axis. In the calculation, grid points inside a sphere of 6 Å radius are employed with grid spacing of 0.3 Å. The gradient correction [18] is included in the exchange-correlation potential. In the calculation, scattering boundary condition is not taken into account, so that all the excited states appear discrete spectrum even above the ionization threshold.

In the upper panels (a-1, 2, 3), an impulsive field is used. In the middle panels (b-1, 2, 3), a static field is abruptly applied at $t = 0$. In the lower panels (c-1, 2, 3), a pulse field with Gaussian envelope is applied. The left three panels (a, b, c-1) show the time profile of the electric field. The middle three panels

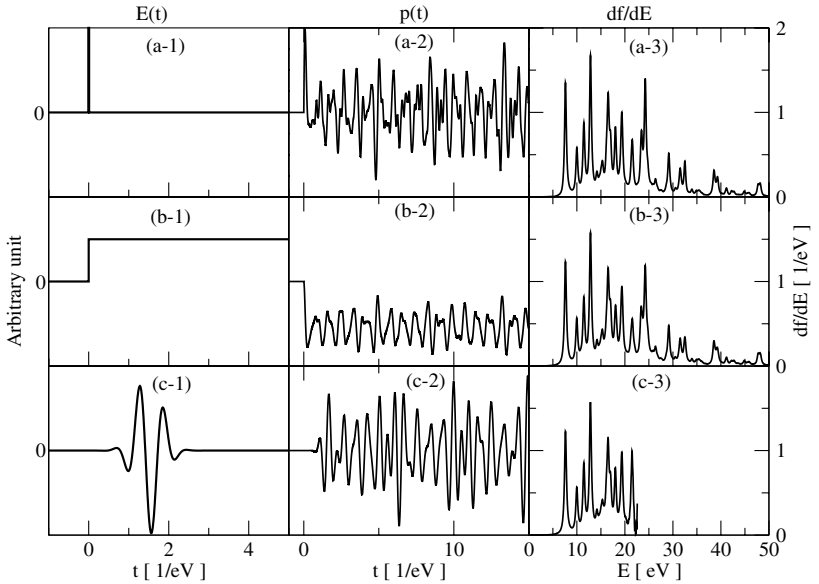

Fig. 1 Real-time optical response calculation for ethylene molecule. The left panels show time profile of three different electric field $E(t)$ applied to the molecule. The middle panels show induced polarization $p(t)$. The right panels show the oscillator strength distribution. See text for more detail.

(a, b, c-2) are induced polarizations. In (a-2), a sharp peak is seen at $t = 0$. Since all electrons are kicked by the impulsive force, all the electrons contribute coherently to the polarization at $t = 0$. In (b-2), the oscillation is seen around negative constant value. Since a constant electric field E_0 is applied at $t > 0$, the oscillation is around the static polarization $p_0 = \alpha(0)E_0$. The right three panels (a, b, c-3) are the oscillator strength distribution which is proportional to the imaginary part of the polarizability multiplied by the frequency, $\mathrm{d}f/\mathrm{d}E \propto \omega\, \mathrm{Im}\, \alpha(\omega)$ with $E = \hbar\omega$. As mentioned in Section 3.3, one may calculate the polarizability for any of the time profiles. The oscillator strength distributions calculated from the three different electric fields indeed coincide to each other. In the calculations of lower three panels (c-1, 2, 3), a pulse of Gaussian envelope, $E(t) = E_0 \cos(\omega_0 t) \exp(-\gamma(t - t_0)^2)$, with $\hbar\omega_0 = 10$ eV, $t_0 = 1.5\hbar$ eV^{-1}, $\gamma = 5$ (eV/$\hbar$)^2 is used. The Fourier transform of this pulse, $\tilde{E}(\omega)$, has an intensity peak at $\hbar\omega_0 = 10$ eV with a width of 5 eV. In contrast to the two electric fields of (a) and (b) which has a sensitivity in full spectral region, the Gaussian pulse (c) has a sensitivity only in the spectral region where $\tilde{E}(\omega)$ is large, below 20 eV.

We next demonstrate the effect of the boundary condition. In Fig. 2, oscillator strength distribution of ethylene molecule is shown in the real-time calculation with absorbing boundary condition (left panel) and in the Green's function method (right panel), which was presented in Ref. [34]. In this calculation, oscillator strength distributions for three Cartesian directions are summed.

In the left panel, the calculations with and without absorbing potential are compared. The dashed line shows result employing grid points inside a sphere of 10 Å without absorbing potential. The solid line shows result employing grid points inside 16 Å, $R = 6$ Å plus $\Delta R = 10$ Å. The strength of the absorbing potential is $W_0 = 4$ eV. The HOMO orbital energy is –11.7 eV in the calculation; thus the strength above 11.7 eV corresponds to photoionization. Below the threshold, both calculations coincide to each other. Above the threshold, the calculated strength without the absorbing potential oscillates due to the reflection of the emitted electrons at the boundary.

In the right panel, the oscillator strength calculated with the Green's function method is compared with measurement [40]. The calculations with the absorbing boundary condition and with the Green's function method coincide to each other to high accuracy. Looking in detail, the oscillator strength in the real-time calculation shows oscillation at around 35 eV which is not seen in the Green's function calculation. This may be caused by an insufficient absorption in the real-time calculation.

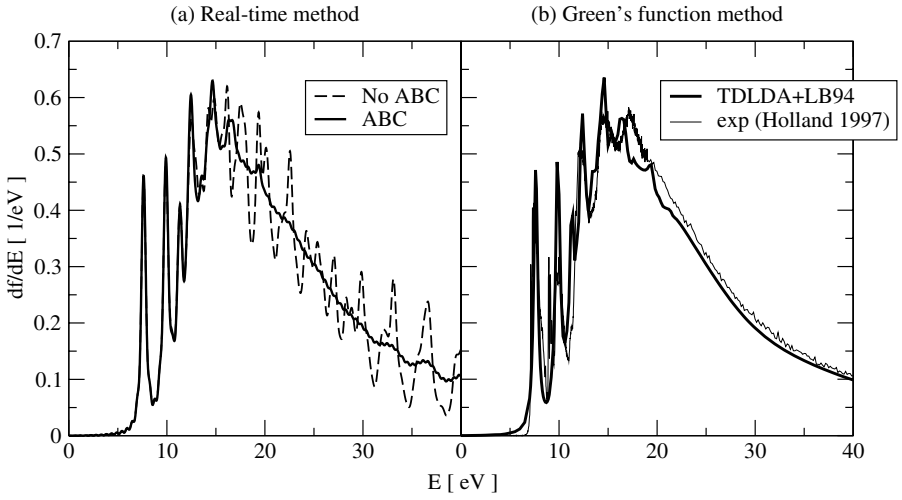

Fig. 2 Oscillator strength distribution of ethylene molecule. The upper panel shows real-time calculation with (bold) and without (thin) absorbing potential. The lower panel show the calculation with the Green's function method and the measurement [40]. The TDDFT calculation is achieved with the gradient correction [18] with the local-density approximation (TDLDA+LB94).

In this example, the oscillator strength is reproduced with high accuracy by the TDDFT calculations. We have calculated optical responses of many other molecules. Some organic molecules are reported in [42]. Photoabsorption of carbon [43] and silver [44] clusters were also investigated. In addition to the photoabsorption, optical activity is investigated in [45]. In Ref. [46], the photoabsorption of structural isomer molecules are analyzed.

6 Real-time, real-space treatment of periodic systems

The optical properties of the bulk periodic system is characterized by the frequency-dependent dielectric function. In this section, we discuss an extension of the real-time method presented in Section 3.3 for infinite periodic systems. In Ref. [47], we discussed this issue starting from a certain Lagrangian appropriate to the problem. We here explain the set of equations stressing a connection with the real-time method for finite systems.

A real-time formalism discussed in Section 3.3 is not directly applicable to infinite periodic systems, since the dipole potential $V_{\rm ext}(\boldsymbol{r},t) = eE(t)r_\nu$ violates the periodicity of the Kohn–Sham Hamiltonian. To recover the periodicity and to apply the Bloch's theorem to TDKS equation, we first make a gauge transformation,

$$\psi_i(\boldsymbol{r},t) = \exp\left\{\frac{ie}{\hbar c}\,A(t)\,r_\nu\right\}\tilde{\psi}_i(\boldsymbol{r},t)\,. \tag{57}$$

Here $A(t)$ is a time-dependent, spatially-uniform vector potential which is related to the external electric field $E(t)$ by $E(t) = -(1/c)\,\mathrm{d}A(t)/\mathrm{d}t$. The TDKS equation with the external electric field $E(t)$ is transformed to

$$i\hbar\frac{\partial}{\partial t}\tilde{\psi}_i(t) = \left\{\frac{1}{2m}\left(\boldsymbol{p} + \frac{e}{c}A(t)\,\hat{r}_\nu\right)^2 + V_{\rm loc}\right\}\tilde{\psi}_i(t) + \mathrm{e}^{-ieA(t)r_\nu/\hbar c}\,V_{\rm nonloc}\,\mathrm{e}^{ieA(t)r_\nu/\hbar c}\,\tilde{\psi}_i(t)\,, \tag{58}$$

where $\hat{r}_\nu$ is a unit vector for ν-direction.

The dipole moment cannot be defined for infinite systems, either. We instead consider a current integrated over the space, which is a time derivative of the dipole moment.

$$\begin{aligned} i_\mu(t) &= \frac{\mathrm{d}}{\mathrm{d}t}p_\mu(t) \\ &= -\frac{e}{m}\sum_i\int \mathrm{d}\boldsymbol{r}\,\psi_i^*(\boldsymbol{r},t)\left(-i\hbar\frac{\partial}{\partial r_\mu}\right)\psi_i(\boldsymbol{r},t) \\ &\quad -i\frac{e}{\hbar}\sum_i\int \mathrm{d}\boldsymbol{r}\,\mathrm{d}\boldsymbol{r}'\,\psi_i^*(\boldsymbol{r},t)\left\{V_{\rm nonloc}(\boldsymbol{r},\boldsymbol{r}')\,r'_\mu - r_\mu V_{\rm nonloc}(\boldsymbol{r},\boldsymbol{r}')\right\}\psi_i(\boldsymbol{r},t)\,, \end{aligned} \tag{59}$$

where we note that the nonlocality of the pseudopotential contributes to the current as given in the last term.

To apply the real-time method to infinite periodic systems, one more thing must be taken into consideration: the surface charge effect. The macroscopic electric field inside a material, $E(t)$, is composed of the external electric field, which is proportional to the electric flux density $D(t)$, and the macroscopic electric field induced by the polarization $P(t)$ at the surface.

$$E(t) = D(t) - 4\pi P(t)\,. \tag{60}$$

Since the polarization at the surface is induced by the current inside a unit cell, we have

$$\frac{\mathrm{d}}{\mathrm{d}t}P(t) = \frac{1}{\Omega}i_\mu(t)\,, \tag{61}$$

where Ω is a volume of the unit cell, and i_μ is defined as an integral of the current over the unit cell of volume Ω. To write up a closed set of equations, we introduce an induced vector potential $A_{\rm ind}(t)$, which is related to the polarization by $P(t) = (1/4\pi c)\,(\partial A_{\rm ind}(t)/\partial t)$. Equation (61) is expressed for $A_{\rm ind}(t)$ as

$$\frac{\partial^2}{\partial t^2} A_{\rm ind}(t) = \frac{4\pi c}{\Omega} i_\mu(t) . \tag{62}$$

The vector potential $A(t)$ in the TDKS Eq. (58) should be a sum of the external one $A_{\rm ext}(t)$, which is related to $D(t)$ by $D(t) = -(1/c)\,(\partial A_{\rm ext}(t)/\partial t)$, and the induced one $A_{\rm ind}(t)$. We now arrive at a closed set of equation, Eq. (58) with $A(t)$ replaced with $A_{\rm tot}(t) = A_{\rm ext}(t) + A_{\rm ind}(t)$, Eq. (62) for the time evolution of the induced vector potential, and Eq. (59) in which the spatial integral should be taken over the unit cell.

As in the calculation of the polarizability, one may calculate the dielectric function $\varepsilon(\omega)$ from real-time Kohn–Sham calculation with external vector potential of any time profile. The dielectric function $\varepsilon(\omega)$ is defined to relate the electric flux density and the total macroscopic electric field of frequency ω, $D_0\, {\rm e}^{-i\omega t} = \varepsilon(\omega)\, E_0\, {\rm e}^{-i\omega t}$. For an electric flux density of any time profile, $D(t)$, Fourier components at frequency ω of $E(t)$ and $D(t)$ are related by the dielectric function,

$$\int {\rm d}t\, {\rm e}^{i\omega t} D(t) = \varepsilon(\omega) \int {\rm d}t\, {\rm e}^{i\omega t}\, E(t) . \tag{63}$$

Expressing in terms of the vector potential, we have an expression which allows us to calculate dielectric function from TDKS solution,

$$\frac{1}{\varepsilon(\omega)} = \frac{\displaystyle\int {\rm d}t\, {\rm e}^{i\omega t}\, \frac{{\rm d}A_{\rm tot}(t)}{{\rm d}t}}{\displaystyle\int {\rm d}t\, {\rm e}^{i\omega t}\, \frac{{\rm d}A_{\rm ext}(t)}{{\rm d}t}} . \tag{64}$$

A simple and useful choice of the external vector potential is a step function, $A_{\rm ext}(t) = A_0\theta(t)$. This corresponds to the impulsive electric field, $E(t) = -(1/c)\,({\rm d}A(t)/{\rm d}t) = -(1/c)\, A_0\, \delta(t)$. Calculation of the dielectric function employing the present formalism is given in [47], taking diamond and Li metal as examples.

7 Summary

In this article, we presented several formalisms of the linear response time-dependent density-functional theory which we have implemented in the three-dimensional uniform grid representation.

For isolated systems, three methods are presented: a real-time method, modified Sternheimer method, and the eigenvalue problem approach. They show their own characteristic in the application. The real-time method is superior to obtain a spectrum of whole spectral region. This is especially suitable for metallic systems where optical responses are dominated by the plasma oscillation which consists of a number of excitations. Modified Sternheimer method is suitable to calculate accurate response for a fixed frequency. Especially, it suits ideally for calculations of nonlinear optical responses. The eigenvalue method is suitable to calculate a few low-lying excitations accurately.

All the methods have a common feature that they do not require construction of the unoccupied Kohn–Sham orbitals. They do not employ a basis function expansion, in contrast to the implementation in the quantum chemistry calculations. The convergence of the calculation may be examined by a relatively simple two parameters, the size of the spatial region and the grid spacing. They also show similar computational aspects: storage requirement scales as the square of the system size. Regarding the computational time, the TDDFT calculations scale as again the square of the system size, once the ground state is constructed. The ground state construction scales as the cube because of the orthogonalization among orbitals. However, the TDDFT calculations do not involve any orthogonalization step.

It is well recognized that the 3D grid representation is suitable for parallel computation with distributed memory systems. The frameworks presented in this article are, therefore, suitable for the implementation in the parallel computation and have a potential usefulness to study electronic excitations of large systems. Study in this direction is now under progress.

Acknowledgement This work is supported by NAREGI Nanoscience Project and by the Grant-in-Aid for Scientific Research (Grant No. 17540231), MEXT, Japan. GFB acknowledges support by the U.S. Department of Energy under grant DE-FG02-00ER41132.

References

[1] E. Runge and E. K. U. Gross, Phys. Rev. Lett. **52**, 997 (1984).
[2] E. K. U. Gross, J. F. Dobson, and M. Petersilka, in: Topics in Current Chemistry, Vol. 181, edited by R. F. Nalewajski (Springer Verlag, Heidelberg, 1996), p. 81.
[3] M. Petersilka and E. K. U. Gross, Laser Phys. **9**, 105 (1999).
[4] F. Calvayrac, P.-G. Reinhard, E. Suraud, and C. A. Ullrich, Phys. Rep. **337**, 493 (2000).
[5] R. Nagano, K. Yabana, T. Tazawa, and Y. Abe, Phys. Rev. A **62**, 062721 (2000).
[6] K. Yabana, T. Tazawa, P. Bozek, and Y. Abe, Phys. Rev. A **57**, R3165 (1998).
[7] K. Yabana and G. F. Bertsch, Phys. Rev. B **54**, 4484 (1996).
[8] J.-I. Iwata, K. Yabana, and G. F. Bertsch, J. Chem. Phys. **115**, 8773 (2001).
[9] C. Jamorski, M. E. Casida, and D. R. Salahub, J. Chem. Phys. **104**, 5134 (1996).
[10] M. E. Casida, C. Jamorski, K. C. Casida, and D. R. Salahub, J. Chem. Phys. **108**, 4439 (1998).
[11] R. E. Stratmann, G. E. Scuseria, and M. J. Frisch, J. Chem. Phys. **109**, 8218 (1998).
[12] R. Bauernschmitt, and R. Ahlrichs, Chem. Phys. Lett. **256**, 454 (1996).
[13] R. Bauernschmitt, M. Häser, O. Treutler, and R. Ahlrichs, Chem. Phys. Lett. **264**, 573 (1997).
[14] S. J. A. van Gisbergen, J. G. Snijders, and E. J. Baerends, Comput. Phys. Commun. **118**, 119 (1999).
[15] S. J. A. van Gisbergen, J. A. Groeneveld, A. Rosa, J. G. Snijders, and E. J. Baerends, J. Phys. Chem. A **103**, 6835 (1999).
[16] S. Hirata and M. Head-Gordon, Chem. Phys. Lett. **302**, 375 (1999).
[17] A. Muta, J.-I. Iwata, Y. Hashimoto, and K. Yabana, Prog. Theor. Phys. **108**, 1065 (2002).
[18] R. van Leeuwen and E. J. Baerends, Phys. Rev. A **49**, 2421 (1994).
[19] A. Zangwill and P. Soven, Phys. Rev. A **21**, 1561 (1980).
[20] W. Ekardt, Phys. Rev. Lett. **52**, 1925 (1984).
[21] J. R. Chelikowsky, N. Troullier, and Y. Saad, Phys. Rev. Lett. **72**, 1240 (1994).
[22] J. R. Chelikowsky, N. Troullier, K. Wu, and Y. Saad, Phys. Rev. B **50**, 11355 (1994).
[23] N. Troullier and J. L. Martins, Phys. Rev. B **43**, 1993 (1991).
[24] L. Kleinman and D. Bylander, Phys. Rev. Lett. **48**, 1425 (1982).
[25] H. Flocard, S. E. Koonin, and M. S. Weiss, Phys. Rev. C **17**, 1682 (1978).
[26] P. Bonche, B. Grammaticos, and S. E. Koonin, Phys. Rev. C **17**, 1700 (1978).
[27] The numerical analysis may be found at: http://gene.phys.washington.edu/~bertsch/ > pedagogical > Comparison of numerical methods...
[28] O. Sugino and Y. Miyamoto, Phys. Rev. B **59**, 2579 (1999).
[29] G. D. Mahan, Phys. Rev. B **22**, 1780 (1980).
[30] S. Baroni, P. Giannozzi, and A. Testa, Phys. Rev. Lett. **58**, 1861 (1987).
[31] Z. H. Levine and D. C. Allan, Phys. Rev. B **43**, 4187 (1991).
[32] M. Stener, P. Decleva, and A. Lisini, J. Phys. B **28**, 4973 (1995).
[33] A. Dal Corso, F. Mauri, and A. Rubio, Phys. Rev. B **53**, 15638 (1996).
[34] T. Nakatsukasa and K. Yabana, J. Chem. Phys. **114**, 2550 (2001).
[35] G. F. Bertsch, A. Schnell, and K. Yabana, J. Chem. Phys. **115**, 4051 (2001).
[36] G. F. Bertsch, J. Giansiracusa, and K. Yabana, Isr. J. Chem. **42**, 151 (2002).
[37] I. Vasiliev, S. Öğüt, and J. R. Chelikowsky, Phys. Rev. Lett. **82**, 1919 (1999).
[38] S. Shlomo and G. Bertsch, Nucl. Phys. A **243**, 507 (1975).
[39] D. Neuhasuer and M. Baer, J. Chem. Phys. **90**, 4351 (1989).
[40] D. M. P. Holland et al., Chem. Phys. **219**, 91 (1997).
[41] M. S. Child, Mol. Phys. **72**, 89 (1991).

[42] K. Yabana and G. F. Bertsch, Int. J. Quantum Chem. **75**, 55 (1999).
[43] K. Yabana and G. F. Bertsch, Z. Phys. D **42**, 219 (1997).
[44] K. Yabana and G. F. Bertsch, Phys. Rev. A **60**, 3809 (1999).
[45] K. Yabana and G. F. Bertsch, Phys. Rev. A **60**, 1271 (1999).
[46] T. Nakatsukasa and K. Yabana, Chem. Phys. Lett. **374**, 613 (2003).
[47] G. F. Bertsch, J.-I. Iwata, A. Rubio, and K. Yabana, Phys. Rev. B **62**, 7998 (2000).

